Variable-Temperature Microelectrode Voltammetry: Application to Diffusion Coefficients and Electrode Reaction Mechanisms

Sarah R. Jacob, Qi Hong, Barry A. Coles, and Richard G. Compton*

Physical and Theoretical Chemistry Laboratory, Oxford University, South Parks Road, Oxford, OX1 3QZ, U.K.

Received: January 4, 1999; In Final Form: February 18, 1999

An apparatus for the measurement of steady-state microelectrode voltammetry at elevated temperatures is described. The scope of this experimental approach as a method for the determination of diffusion coefficients at variable temperatures in the case of simple one-electron processes is demonstrated. Diffusion coefficients over a range of temperatures are derived for *N*,*N*,*N*′,*N*′-tetramethylphenylenediamine in both acetonitrile and water solvents, tris-4-bromophenylamine in acetonitrile, and ferrocene in acetonitrile and dimethylformamide from which activation energies for diffusion are obtained. Diffusion coefficient values are used to derive Stokes−Einstein radii for each species in solution. The electroreductions of *o*-bromonitrobenzene in dimethylformamide and 9-chloroanthracene in acetonitrile are studied as a function of temperature and activation energies estimated for carbon−halide bond cleavage in the corresponding radical anions.

1. Introduction

There is considerable current interest in the use of high- and/or variable-temperature measurements for the study of dynamic electrochemical problems by a range of groups. First, Ross and co-workers[1,2] have made use of rotating disk electrode measurements in the range 293−333 K to provide insights into the electroreduction of oxygen and the hydrogen evolution reaction by measuring the temperature dependence of the current−voltage curves obtained at different low-index crystal faces of platinum. The inference of activation energies, heats of adsorption, and the temperature dependence of Tafel plots allowed new and unique mechanistic insights into familiar and much-studied processes. Second, Grundler has pioneered a hot wire experiment in which ac heating is used simultaneously with dc polarization to permit electrolysis in aqueous solutions brought near their boiling points.[3−6] The oxidations of simple organic molecules including formaldehyde, methanol, formic acid, and glucose were studied in aqueous solution and self-poisoning effects were seen to be alleviated at temperatures of ca. 79 °C,[3] and in a separate study, the merits of elevated temperatures in the determination of As and Hg by stripping voltammetry were noted.[7] Last, Corti and Calvo have designed a high-temperature wall-tube cell and reported the effects of temperature on transport properties up to 142 °C,[8] while Bard[10] has used microdisk electrodes for similar purposes. These and earlier[10−12] studies hint at the importance of adopting temperature as a routine variable in mechanistic and analytical electrochemistry.

In this paper, we introduce an experimental approach to allow steady-state microelectrode voltammetry at elevated and variable temperatures. For ease of manipulation, the apparatus employs rapid temperature control to successively higher values up to 100 °C while ensuring that the electrolytic solution is maintained at an accurate and stable temperature over the time scale required for the acquisition of steady-state data. In addition, we describe applications of this technique first as a method of determining diffusion coefficients at elevated temperatures as applied to ferrocene,[13] *N*,*N*,*N*′,*N*′-tetramethylphenylenediamine[14−18] (TMPD), and tris(*p*-bromophenyl)amine[19−21] (TBPA) in a range of solvent media. All three species are known to undergo oxidation via a simple one-electron transfer without mechanistic complication. Diffusion coefficients at elevated temperatures are used in the determination of activation energies for diffusion, and the variation of the diffusion coefficient with temperature is compared to the predicted correlation according to the Wilke−Chang relationship.[22] Second, we describe application of this technique in the determination of activation parameters for the halide bond cleavage of *o*-bromonitrobenzene and 9-chloroanthracene. Both species undergo rapid halide bond cleavage via a two-electron transfer process probably via an ECE-type process.[23−37]

2. Elevated Temperature Microelectrode Apparatus

The electrolytic cell of the variable-temperature apparatus is shown in Figure 1. It comprises a Pyrex (borosilicate) glass tube 20 cm in length and 0.7 mm in diameter with electrodes positioned at one end. Microdisk electrodes with an overall diameter of 5 mm are sealed into one end of the heated unit by means of silicone rubber tubing as shown in Figure 1. Electrodes were made by sealing platinum wire with a diameter ranging between 5 and 50 μm into a soda-glass capillary housing using a hand torch. The application of sufficient heat caused the glass to soften until it collapsed onto the platinum wire. Electrodes were ground using a diamond wheel to expose the cross section of the embedded wire and subsequently polished using aqueous alumina slurries to obtain a flat surface. Grades of 9 μm and 3 μm applied directly to a glass surface were used initially followed by 1 μm and 0.3 μm grades supported on a soft nap (PSU-S) lapping pad (Kemet International Ltd., Maidstone, Kent).

The reference electrode comprises a platinum wire positioned inside the heated unit close to the microelectrode. The platinum wire is sealed into the heated unit via a Pyrex arm and soldered to a brass cap at the top of the arm which serves as an external electrical contact. The counter electrode consists of a platinum coil which surrounds the glass housing of the microelectrode. Positioning of the counter electrode downstream of the working

* Corresponding author.

10.1021/jp990024w CCC: $18.00
Published on Web 03/26/1999

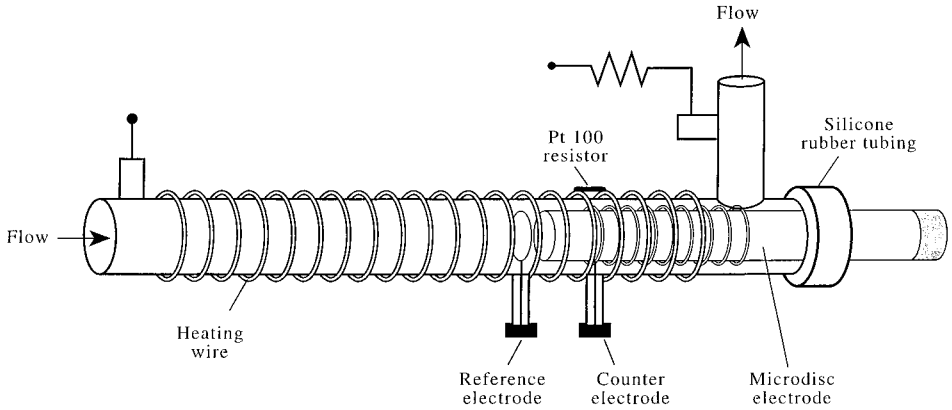

Figure 1. Variable-temperature apparatus.

electrode surface ensures that unwanted counterproducts are removed without contact with the microelectrode by flow of the solution to waste. For the reference electrode, the wire is sealed into the cell and external electrical contact made via a sidearm on the heated unit.

Heat is supplied to the voltammetric unit by means of heating wire coiled around the glass tube. The heating wire comprises manganin wire insulated with an epoxy cement (supplied by Johnson Matthey, Reading, Berks, UK). Heating wire is bonded to the Pyrex unit using epoxy varnish (supplied by Gittings and Hill Ltd., Birmingham, UK). The tubelike structure of the heated unit provides a large surface area-to-volume ratio, thereby allowing rapid and accurate heating of the electrolytic solution within. Power input to the wire is controlled by a PID controller (an Autotune Temperature Controller, model CAL3200, supplied by CAL Controls Ltd., Hitchin, Herts., UK) connected to a Pt100 sensor located adjacent to the heating wire. Temperature stability of the control system as observed by fluctuation of the temperature around the set point is 0.1 °C at 30 °C rising to 0.3 °C at 95 °C.

A flow of solution is maintained through the heated cell during the course of experimental work so as to maintain a fresh supply of electrolytic solution at the electrode surface and to ensure the removal of waste products. Solution is delivered to the unit via gravity flow from a 500 cm^3 glass reservoir. The reservoir comprises a round-bottomed vessel with one large inlet and two small inlet arms. The bottom of the vessel contains a glass exit tube through which solution flows to reach the voltammetric cell. One of the small inlet arms contains a pipet connected to a supply of argon gas thereby facilitating solution deoxygenation. Argon gas is bubbled through the solution for 30 min prior to use and throughout the experimental procedure. The gap between the pipet and inlet arm is sealed using Parafilm. In addition, the electrolytic solution is heated during the degassing procedure to a temperature of 40 °C using a heating mantle placed around the reservoir. This serves to remove dissolved gas present in the solution which at higher temperatures becomes less soluble in the solution to form gas bubbles. In this way, the formation of bubbles in the flow cell during elevated-temperature work is avoided. A thermometer is placed into the remaining small inlet arm and sealed into place using Parafilm.

The flow of solution from the reservoir to the heated unit and subsequently to waste is shown schematically in Figure 2. Upstream of the cell, the flow system is composed principally of glass where possible and Teflon tubing where greater flexibility is required so as to minimize the ingress of oxygen into the solution. The flow system between the reservoir and cell incorporates a length of glass tubing connected to a 20 cm

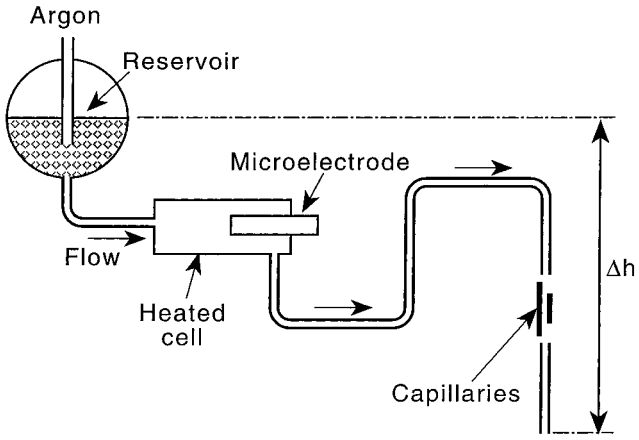

Figure 2. Schematic diagram showing the elevated-temperature cell incorporated into a flow system.

length of Teflon which is then joined to the heated cell. The remainder of the flow system comprises a length of Teflon tubing running from the cell to a glass capillary system. After exiting the capillary system, solution flows through a length of Teflon tubing to a glass tip where it drips into a waste receptacle. Connections are made using silicone rubber tubing. Since silicone rubber tubing is permeable to oxygen, connections upstream of the electrode are jacketed with plastic bags containing a positive pressure of nitrogen to exclude oxygen. The length of Teflon tube upstream of the heating cell is also jacketed using a nitrogen-filled plastic bag.

Control of flow rate is achieved via the system of calibrated capillary tubes, constructed of Pyrex glass, which form part of the outlet flow system. Capillaries are of identical bore size but differ in length; thus, flow rate can be varied with the capillary selected. In addition, a bypass tube is present to enable rapid flow of solution as a means of filling and emptying the cell and also to facilitate bubble removal. Selection of the capillary or bypass is made using a valve. Calibration of flow rate for each capillary for a range of solvents was carried out in terms of the height difference between the outlet tube and the reservoir level as denoted by Δh in Figure 2. A flow rate of approximately 7×10^{-3} cm^3 s^{-1} was maintained throughout most experimental investigations. The possible enhancement of limiting current as a result of forced convection at the electrode surface was assessed by comparison of the limiting currents obtained for the oxidation of a standard 1 mM ferrocene/acetonitrile/0.1 M tetrabutylammonium perchlorate solution in the presence and absence of flow using a 10 μm microdisk electrode. No change was observed indicating that for a flow rate of 7×10^{-3} cm^3 s^{-1}, steady-state currents can be regarded

as diffusion-limited for microelectrodes of 10 μm diameter or smaller. The temperature stability of the solution at this flow rate was measured by positioning a Pt100 sensor at the site of the working electrode. Temperature stability as measured by fluctuation of the solution temperature around the set point over a 30 min period was 0.3 °C at 30 °C rising to 1.0 °C at 95 °C.

Linear sweep functions and current measurement are performed using a linear sweep potential scan generator attached to a picoammeter. This is controlled by a model 486 personal computer with 66 MHz clock speed using data acquisition software which allows for linear sweep scan rates in the range 5 mV s^{-1} to 1 V s^{-1} and acquisition of the resulting current−voltage curves obtained. Analysis of data obtained in computerized format is performed using a data analysis program which permits measurement of limiting currents and half wave potentials. In addition, analysis of the steady-state current−voltage curves in terms of the diagnostic test for electrochemical reversibility is also possible.

The voltammetric investigation of *o*-bromonitrobenzene (oBNB) and ferrocene in dimethylformamide (DMF) solution and 9-chloroanthracene (9-ArCl), ferrocene, TMPD, and TBPA in acetonitrile solution was conducted using 0.1 M tetrabutylammonium perchlorate (TBAP) as a supporting electrolyte. Acetonitrile (Fisons, >99.99% purity) and DMF (Aldrich, HPLC grade) were dried prior to use via passage through an alumina column and run directly into the reaction vessel under a stream of argon gas. The study of TMPD in aqueous solution used UHQ water with a measured resistivity of 18 MΩ cm achieved using an Elgastat (High Wycombe, Bucks) water purifier. The supporting electrolyte comprised 0.1 M potassium chloride (KCl). NBu_4ClO_4 (Fluka, >99% purity), KCl (Aldrich, 99% purity), TMPD (Aldrich, 99% purity), TBPA (Aldrich, 99% purity), ferrocene (Aldrich, 99% purity), oBNB (Aldrich, 98% purity), and 9-ArCl (Lancaster, 97% purity) were used as received. Platinum microelectrodes with nominal diameters of 5 μm were used for investigations of 9-ArCl, TMPD, TBPA, and ferrocene in acetonitrile. A microelectrode of 10 μm was used for the study of oBNB and ferrocene in DMF. Precise electrode dimensions were determined via electrochemical calibration using a standard 1 mM ferrocene/acetonitrile/0.1 NBu_4ClO_4 solution. Electrodes were polished prior to use with a 0.3 μm alumina slurry supported on a soft nap lapping pad. Voltammograms were recorded at temperatures ranging between 24 and 60 °C and between 30 and 80 °C for investigations conducted in acetonitrile or DMF and water, respectively, with an accuracy ±0.5 °C.

3. Results and Discussion

3.1. Diffusion Coefficients. The one-electron oxidations of ferrocene, TMPD, and TBPA were studied in acetonitrile/0.1M TBAP solution using a platinum microdisk electrode over the temperature range 25−80 °C. Measured half wave potentials at 25 °C were in good agreement with literature values. Diffusion coefficients were determined from transport limited currents, I_{lim}, via the equation

$$I_{lim} = 4nFD[X]r \qquad (1)$$

where n denotes the number of electrons transferred, F is the Faraday constant, [X] is the bulk concentration of the electrosensitive species, D its diffusion coefficient, and r the electrode radius. Values of diffusion coefficents at 25 °C were in good agreement with independent reports for all three species.[13−21] Table 1 summarizes the temperature dependence of the diffusion coefficients. Next, the oxidation of ferrocene in DMF/0.1 M TBAP was examined. A half wave potential of 0.2 V (vs Pt pseudoreference electrode) was observed. Diffusion coefficients obtained at temperatures ranging between 25 and 45 °C are given in Table 2. Finally, the temperature dependence of the oxidation of TMPD in water was investigated. At 25 °C, a half wave potential of +0.1 V (vs Pt pseudoreference electrode) was observed. The measured diffusion coefficients are summarized in Table 3.

TABLE 1: Temperature Dependence of Diffusion Coefficients in Acetonitrile

temp/°C	D/cm^2 s^{-1}
(a) Ferrocene	
24	$2.37 \times 10^{-5} \pm 1.0 \times 10^{-6}$
30	$2.51 \times 10^{-5} \pm 1.0 \times 10^{-6}$
40	$2.72 \times 10^{-5} \pm 1.1 \times 10^{-6}$
50	$2.98 \times 10^{-5} \pm 1.2 \times 10^{-6}$
60	$3.20 \times 10^{-5} \pm 1.3 \times 10^{-6}$
(b) Tetramethylphenylenediamine	
23.5	$2.39 \times 10^{-5} \pm 0.9 \times 10^{-6}$
30	$2.61 \times 10^{-5} \pm 1.0 \times 10^{-6}$
40	$2.96 \times 10^{-5} \pm 1.2 \times 10^{-6}$
50	$3.33 \times 10^{-5} \pm 1.3 \times 10^{-6}$
60	$3.73 \times 10^{-5} \pm 1.5 \times 10^{-6}$
(c) Tris(*p*-bromophenyl)amine	
22	$1.50 \times 10^{-5} \pm 0.6 \times 10^{-6}$
30	$1.66 \times 10^{-5} \pm 0.7 \times 10^{-6}$
40	$1.83 \times 10^{-5} \pm 0.7 \times 10^{-6}$
50	$2.05 \times 10^{-5} \pm 0.8 \times 10^{-6}$
60	$2.24 \times 10^{-5} \pm 0.9 \times 10^{-6}$

TABLE 2: Temperature Dependence of the Ferrocene Diffusion Coefficient in DMF

temp/°C	ferrocene D/cm^2 s^{-1}
24.8	$1.07 \times 10^{-5} \pm 0.4 \times 10^{-6}$
30	$1.18 \times 10^{-5} \pm 0.5 \times 10^{-6}$
35	$1.30 \times 10^{-5} \pm 0.5 \times 10^{-6}$
40	$1.43 \times 10^{-5} \pm 0.6 \times 10^{-6}$
45	$1.55 \times 10^{-5} \pm 0.6 \times 10^{-6}$

TABLE 3: Temperature Dependence of the Diffusion Coefficient of Tetramethylphenylenediamine in Aqueous 0.1 M KCl

temp/°C	D/cm^2 s^{-1}
30	$6.32 \times 10^{-6} \pm 0.3 \times 10^{-6}$
40	$7.94 \times 10^{-6} \pm 0.3 \times 10^{-6}$
50	$9.99 \times 10^{-6} \pm 0.4 \times 10^{-6}$
60	$1.22 \times 10^{-5} \pm 0.5 \times 10^{-6}$
70	$1.49 \times 10^{-5} \pm 0.6 \times 10^{-6}$
80	$1.86 \times 10^{-5} \pm 0.7 \times 10^{-6}$

The data in Tables 1−3 were analyzed in terms of the Arrhenius equation,

$$D = D_0 e^{-E_a/RT} \qquad (2)$$

where E_a is the activation energy for diffusion of the substrate of interest in the pertinent solvent. Figure 3 shows the five systems studied analyzed in the form of ln D against 1/T plots. Using Figure 3b, E_a for the diffusion of TMPD in acetonitrile was determined to be 10.0 ± 0.8 kJ mol^{-1}. This is in good agreement with values of 10 kJ mol^{-1} [15] and 11 kJ mol^{-1} [38] reported by Zon et al. for the E_a for diffusion of TMPD in an identical solvent medium. Activation energies for the diffusion of ferrocene and TBPA in acetonitrile were determined to be 6.9 ± 0.7 and 8.7 ± 0.7 kJ mol^{-1} using parts a and c of Figure 3, respectively. The activation energy required for diffusion of each species in acetonitrile solution is similar, as expected. The

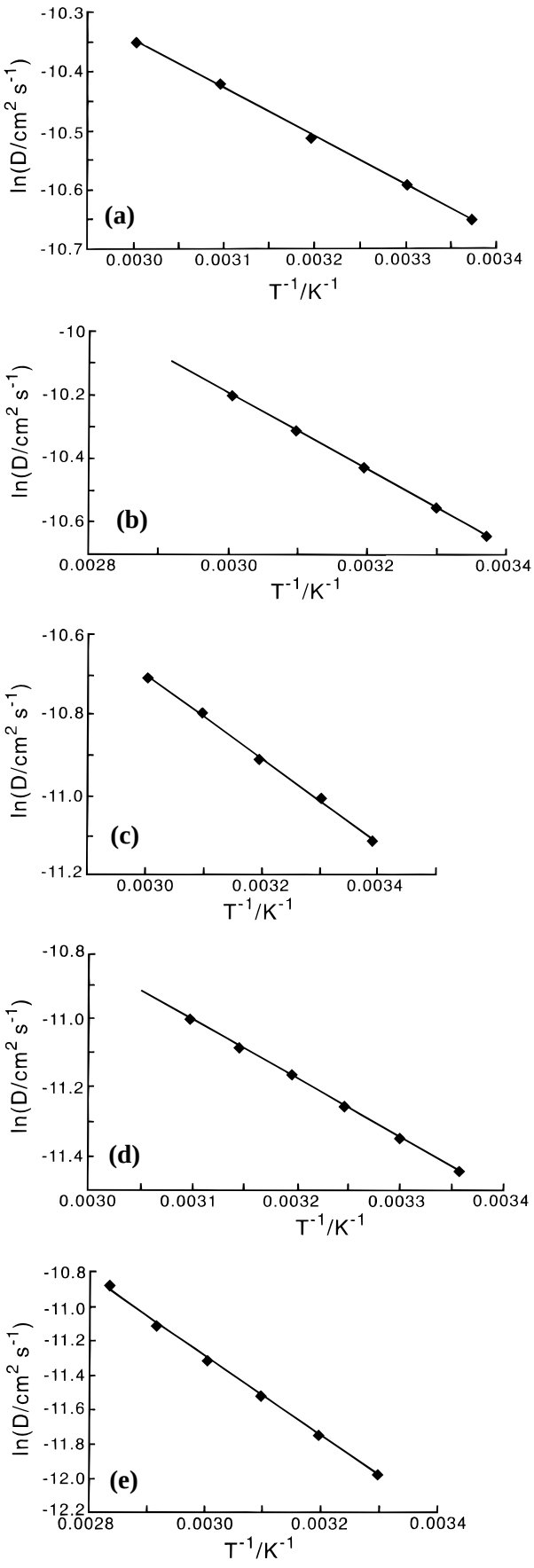

Figure 3. Arrhenius plots for the data summarized in Tables 1−3: (a) ferrocene/acetonitrile; (b) TMPD/acetonitrile; (c) TBAP/acetonitrile; (d) ferrocene/DMF; (e) TMPD/H_2O.

activation energy for the diffusion of ferrocene in DMF was derived as 14.4 ± 1.2 kJ mol^{-1} on the basis of the Arrhenius plot shown in Figure 3d. This reflects the increased viscosity of the DMF solvent in comparison to acetonitrile.[39,40] Figure 3e yielded a value of 19.0 ± 1.5 kJ mol^{-1} for the E_a required for diffusion of TMPD in water. This value is almost twice that observed for diffusion of the same and other species in acetonitrile. This can be attributed to the high viscosity of water.[39,40]

The Wilke−Chang relationship has been proposed as a means of estimating diffusion coefficients of species in solution[41] where D is given by

$$D = 7.4 \times 10^{-8} \frac{(\chi M)^{1/2} T}{\nu V^{0.6}} \tag{3}$$

in which M is the molecular weight of the solvent and V is the molal volume of the solute at normal boiling point estimated for complex molecules by atomic contributions as defined by Perry.[42] χ is an association parameter equal to 2.6 in the case of water and 1 for nonassociated solvents. Development of the theory was based on empirical observation, and for most of the systems studied, a correlation to within 10% of the experimentally determined diffusion coefficient was observed.

The available tabulations of molal volumes permit Wilkie−Chang estimates to be made for the diffusion coefficients of TMPD and TBPA and their temperature dependence. This is shown in Figure 4 together with the experimentally determined values. Note that in calculating the former the temperature dependence of the viscosity was incorporated using literature sources.[39,42] The figures show poor agreement both in absolute values and in the temperature dependence. The applicability of the Wilkie−Chang correlation to these "flat" molecules appears to be questionable.

Last, we note that the approximately linear plots of D against T given in Figure 4 are consistent with the Stokes−Einstein relationship:

$$D = \frac{kT}{w\pi\nu a} \tag{4}$$

where k is the Boltzmann constant, ν corresponds to solution viscosity, a defines the molecular radius, and w corresponds to a constant dependent on the behavior of the diffusing particle. The parameter w is defined by two boundary conditions corresponding to "slip" and "stick" behavior where w is equivalent to 4 and 6, respectively. "Stick" behavior occurs when the species is surrounded by a layer of solvent molecules which move with the diffusing molecule. In the "slip" boundary condition, the diffusing species moves independently of the solvent.

From the plot of D versus T/ν for TMPD in acetonitrile, effective radii of 0.25 and 0.37 nm were calculated using Stokes−Einstein coefficents of 6 and 4, respectively. This is in excellent agreement with values reported by Fernández and Zon.[14] For TMPD in water, effective radii of 0.37 and 0.554 nm were derived assuming Stokes−Einstein coefficients of 6 and 4, respectively. Using the Stokes−Einstein relationship and values of w of 6 or 4, effective radii of 0.25 or 0.37 nm for TMPD in acetonitrile can be estimated. The corresponding values in water are 0.37 and 0.55 nm. For TBPA in acetonitrile radii of 0.46 or 0.69 nm can be estimated.

3.2. Electrode Reaction Mechanisms. We consider first the reduction of *o*-bromonitrobenzene in DMF solution studied in the temperature range 25−45 °C. A representative voltammo-

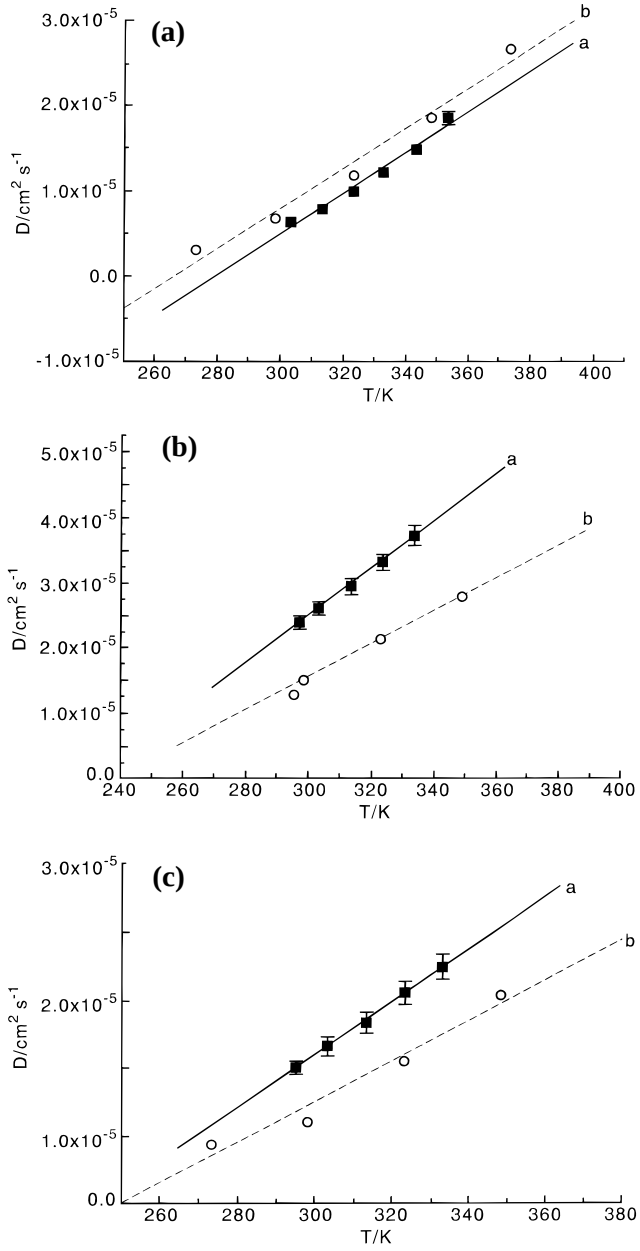

Figure 4. Temperature dependence of the diffusion coefficient of (a) TMPD/H_2O, (b) TMPD/acetonitrile, and (c) TBPA/acetonitrile. The solid line shows experiments, the dashed line the calculated Wilkie−Chang behavior.

gram obtained for the reduction of oBNB at a 5 μm platinum microdisk electrode at 25 °C is shown in Figure 5. Oxidation of ferrocene under similar conditions is observed at a half wave potential ($E_{1/2}$) of +0.2 V versus the platinum pseudoreference electrode. A single wave was observed for the reduction of oBNB with an $E_{1/2}$ of −1.18 V versus the ferrocene/ferrocenium (Fc/Fc^+) couple. The $E_{1/2}$ value obtained is in good agreement with values reported for the reduction of oBNB in an identical solvent medium by others.[30,32,37] Limiting currents obtained for the reduction of oBNB and oxidation of ferrocene at each temperature are summarized in Table 4. The observed single reduction wave for oBNB is consistent with the following ECE-type mechanism:

$$\text{oBNB} + \text{e} \leftrightarrow [\text{oBNB}]^{\bullet -} \qquad \text{(i)}$$

$$[\text{oBNB}]^{-} \rightarrow \text{Br}^{-} + {}^{\bullet}\text{C}_6\text{H}_4\text{NO}_2 \qquad \text{(ii)}$$

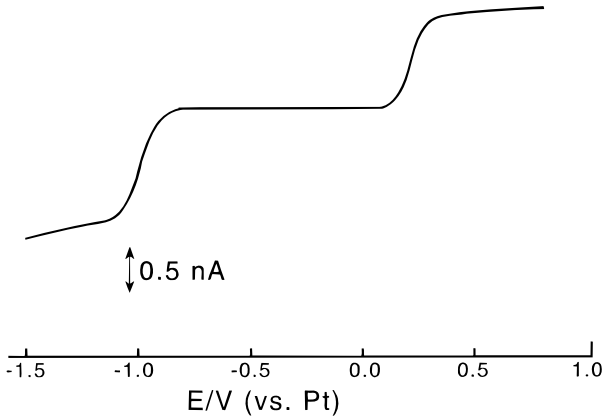

Figure 5. Microdisk voltammogram for the reduction of oBNB in DMF.

$$^{\bullet}\text{C}_6\text{H}_4\text{NO}_2 + \text{e} \xrightarrow{\text{HS}} [\text{C}_6\text{H}_5\text{NO}_2]^{\bullet -} \qquad \text{(iii)}$$

in which the hydrogen atom which substitutes the bromine in the starting material is derived from the solvent/supporting electrolyte system, HS. Such ECE processes are readily kinetically characterized by the "effective" number of electrons transferred in the electrode process, n_{eff}. That is the ratio of current flowing in processes (i) and (iii) to that passing in step (i) alone. Clearly, n_{eff} varies between 1 and 2 as either k increases or the rate of mass transport decreases. An approximate expression has been derived for this behavior,[43]

$$\frac{1}{(n_{\text{eff}} - 1)} = \frac{4}{\pi}\left(\frac{D}{k}\right)^{V_3}\frac{1}{r} + 1 \qquad (5)$$

where r is the disk radius and D the diffusion coefficient of oBNB. It follows that measurements of n_{eff} permit the deduction of values of k if D is known. In the case of oBNB both the determination of n_{eff} and D is problematic since step (iii) occurs at more positive potentials than required for step (i) so that the size of the single voltammetric wave and its variation with temperature reflects both the magnitude of, and changes in, D and r. Accordingly, we use the following protocol to deconvolute the required information from the voltammetric data. First, the activation energy for diffusion in DMF was determined above to be 14.4 kJ mol^{-1}. Second, we note that the diffusion coefficient of oBNB has been measured[30] at 25 °C under a mass transport regime where the reaction goes fully to completion ($n_{\text{eff}} \rightarrow 2$). This observation enables us to use eq 2 to estimate D as a function of temperature; the results are summarized in Table 4. Third, n_{eff} at each temperature can be directly obtained as the ratio of the experimentally determined current to the theoretically predicted current for the one-electron reduction of oBNB as recorded in Table 4. Rate constants for the halide bond cleavage of oBNB subsequently calculated using eq 5 are also shown in Table 4. The rate constant (k) at room temperature correlates favorably with literature values.[30,31]

In a separate investigation we used microelectrodes of variable radii to confirm a value for the rate of oBNB halide bond cleavage at room temperature. Limiting currents obtained for each electrode diameter are shown in Table 5. Using the literature value of D for oBNB in an identical solvent medium at 25 °C,[9] limiting currents for the one-electron reduction of oBNB at each electrode diameter were calculated using eq 1 and are tabulated in Table 5. Values of n_{eff} were then obtained by ratio of the experimentally determined limiting current to the predicted one-electron reduction current as also shown in

TABLE 4: Experimentally Determined and Calculated Parameters for the Reduction of 1 mM oBNB in DMF/0.1 M NBu_4ClO_4 Solution at a 5 μm Diameter Microelectrode

temp/°C	ferrocene I_{lim}/A	oBNB I_{lim}/A	estimated oBNB D/ cm^2 s^{-1}	estimated I_{lim} for oBNB one-electron reduction/A	N_{eff}	k/s^{-1}
24.8	1.10×10^{-9}	1.33×10^{-9}	8.77×10^{-6}	9.05×10^{-10}	1.47	170 ± 20
30	1.22×10^{-9}	1.53×10^{-9}	9.69×10^{-6}	1.00×10^{-9}	1.54	315 ± 40
35	1.34×10^{-9}	1.72×10^{-9}	1.06×10^{-5}	1.10×10^{-9}	1.56	423 ± 50
40	1.47×10^{-9}	1.94×10^{-9}	1.16×10^{-5}	1.20×10^{-9}	1.62	740 ± 90
45	1.59×10^{-9}	2.17×10^{-9}	1.27×10^{-5}	1.31×10^{-9}	1.66	1175 ± 150

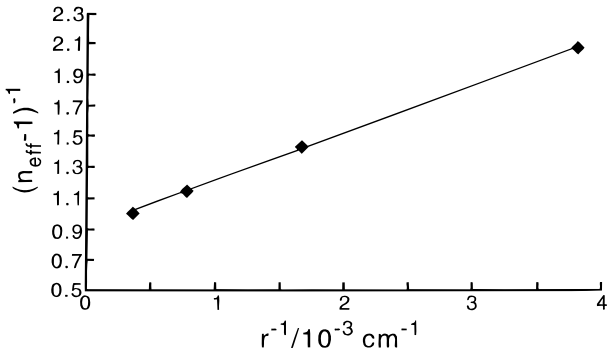

Figure 6. Analysis of the microdisk current data measured for different electrode radii (r) for oBNB in terms of an ECE mechanism (see text).

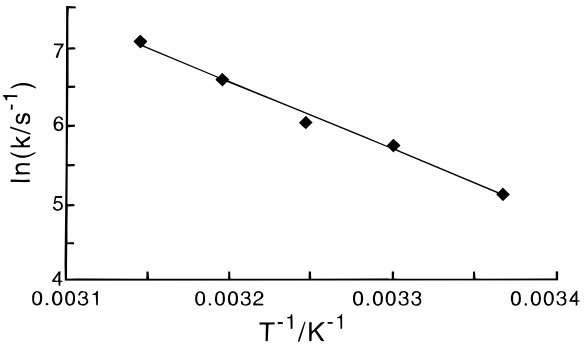

Figure 7. Arrhenius plot for the C−Br bond cleavage in the reduced anion of oBNB.

TABLE 5: Experimentally Determined and Calculated Parameters for the Reduction of 1 mM oBNB in DMF/0.1 M NBu_4ClO_4 Solution at Microelectrodes of Variable Diameter at 25 °C

electrode diameter (μm)	experimentally determined I_{lim} (A)	Calculated I_{lim} for the one-electron reduction of oBNB (A)	N_{eff}
5	1.36×10^{-9}	9.22×10^{-10}	1.48
10	3.55×10^{-9}	2.10×10^{-9}	1.69
25	8.47×10^{-9}	4.52×10^{-9}	1.87
50	1.98×10^{-8}	9.92×10^{-9}	2.00

Table 5. Using the theory of Fleischmann et al. in eq 5 to describe the variation of limiting current with electrode radius for an ECE process, a plot of $1/\Delta n$ versus $1/r$ permits the deduction of values of k. n_{eff} values were used to construct the plot of $1/\Delta n$ versus $1/r$ shown in Figure 6. From this, the rate constant for halide bond cleavage of oBNB at 25 °C was determined to be 148 ± 30 s^{-1}, in good agreement with our previous value derived using the variable temperature apparatus.

Values of k reported in Table 4 were used to construct the Arrhenius plot of ln k versus $1/T$ shown in Figure 7 from which activation parameters for the halide bond cleavage of oBNB were evaluated. 71 ± 7 kJ mol^{-1} and 5.83×10^{14} s^{-1} were obtained for E_a and the preexponential factor A, respectively. The preexponential factor is related to a change in entropy undergone by the reactant species during the activation process. For a first-order reaction, this is defined by eq 6[44],

$$A = \ln \frac{kTe}{h} + \frac{\Delta S_{298}^{\mp}}{R} \qquad (6)$$

in which k is the Boltzmann constant, h is Planck's constant, R is the gas constant, and $\Delta S_{298}^{\mp}$ defines the entropy change undergone by the reactant species. Using this relationship, the entropy of activation for halide bond cleavage of oBNB was calculated to be $+29.4 \pm 3$ J K^{-1} mol^{-1}. The good linear Arrhenius plot shown in Figure 7 confirms the general strategy proposed for interpretation of the voltammetric data.

We next consider the reduction of 9-chloroanthracene in acetonitrile solution in the temperature range 24−60 °C. A representative voltammogram obtained for the reduction of 9-ArCl at 24 °C is shown in Figure 8. Reduction of 9-ArCl is observed at an $E_{1/2}$ value of −2.18 V versus the Fc/Fc$^+$ couple, consistent with the value reported at 25 °C by Wipf and

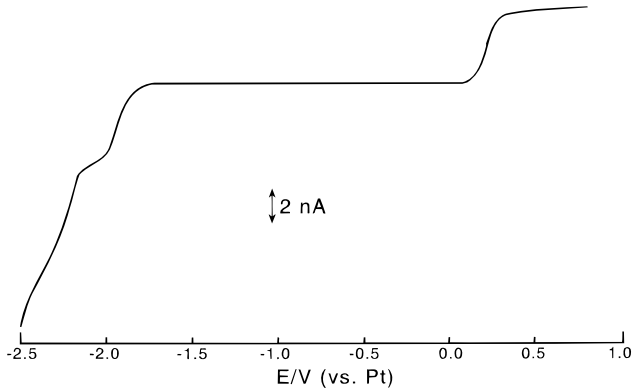

Figure 8. Microdisk voltammogram for the reduction of 9-ArCl in acetonitrile.

TABLE 6: Experimentally Determined and Calculated Parameters for the Reduction of 1 mM 9-ArCl in Acetonitrile/0.1 M $NBu4ClO_4$ Solution at a 10 μm Diameter Microelectrode

temp/°C	ferrocene I_{lim}/A	9-ArCl I_{lim}/A	estimated 9-ArCl D/cm^2 s^{-1}	estimated I_{lim} for 9-ArCl one-electron reduction/A	N_{eff}	k/s^{-1}
24	4.33×10^{-9}	4.24×10^{-9}	1.61×10^{-5}	2.67×10^{-9}	1.59	278 ± 35
30	4.59×10^{-9}	4.61×10^{-9}	1.71×10^{-5}	2.83×10^{-9}	1.63	422 ± 50
40	4.97×10^{-9}	5.19×10^{-9}	1.87×10^{-5}	3.09×10^{-9}	1.68	781 ± 95
50	5.44×10^{-9}	5.80×10^{-9}	2.02×10^{-5}	3.35×10^{-9}	1.73	1212 ± 150
60	5.84×10^{-9}	6.46×10^{-9}	2.18×10^{-5}	3.61×10^{-9}	1.79	2592 ± 310

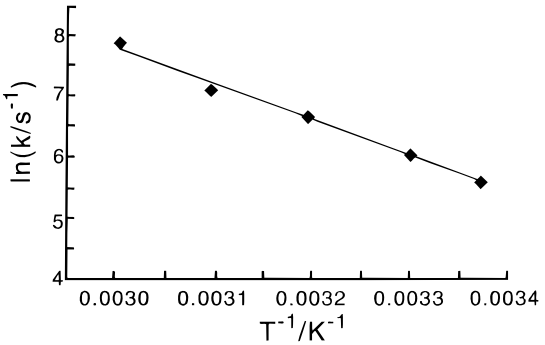

Figure 9. Arrhenius plot for the C−Cl bond cleavage in the radical anion of 9-ArCl.

Wightman.[2−7] Limiting currents for the oxidation of ferrocene and the first reduction wave of 9-ArCl at each temperature are tabulated in Table 6.

Rate constants were obtained using an analogous procedure to that outlined above for oBNB but using the activation energy for transport in acteonitrile deduced above. Values of D, the theoretical limiting current for the one-electron reduction of 9-ArCl, n_{eff}, and k at each temperature are recorded in Table 6. k at room temperature was observed to be in reasonable agreement with values of k for halide bond cleavage of 9-ArCl in the same solvent medium, namely, 200, 260, and 165 s^{-1} reported by Wipf and Wightman,[27] M'Halla et al.,[33] and Jaworski et al.,[34] respectively.

The Arrhenius plot constructed from the values of k reported in Table 6 is shown in Figure 9. From this, values of $+48.7 \pm 4$ kJ mol^{-1} and $+7.98 \times 10^9$ s^{-1} were obtained for E_a and the preexponential factor A, respectively. Using eq 6, the entropy of activation for halide bond cleavage of 9-ArCl was calculated to be -42 ± 4 J K^{-1} mol^{-1}. Activation parameters for the halide bond cleavage of 9-ArCl have previously been derived in DMF. Values of +46, +57. 3, and +63.6 kJ mol^{-1} were obtained for the activation energy by Savéant et al.,[28] Savéant et al.,[35] and Parker[36] using rapid scan cyclic voltammetry, double potential step chronoamperometry, and derivative cyclic voltammetry, respectively. Corresponding activation entropies were −59.0, −16.7, and −0.4 J K^{-1} mol^{-1}.

Conclusions

The apparatus described permits quantitative kinetic and mechanistic investigation of electrode reaction mechanisms over a variable range of temperatures. Data for diffusion coefficients and rate constants is readily measurable and interpreted.

Acknowledgment. We thank EPSRC and Shell for a CASE studentship for S.R.J.

References and Notes

(1) Grgu, B. N.; Markovic, N. M.; Ross, P. N. *Can. J. Chem.* **1997**, *75*, 1465.
(2) Markovic, N. M.; Grgu, B. N.; Ross, P. N. *J. Phys. Chem. B* **1997**, *101*, 5405.
(3) Zerihun, T.; Grundler, P. *J. Electroanal. Chem.* **1998**, *441*, 57.
(4) Grundler, P.; Kirbs, A.; Zerihun, T. *Analyst* **1996**, *121*, 1805.
(5) Zerihun, T.; Grundler, P. *J. Electroanal. Chem.* **1996**, *415*, 85.
(6) Zerihun, T.: Grundler, P. *J. Electroanal. Chem*. **1996**, *404*, 243.
(7) Flechsig, G. U.; Jasinski, M.; Grundler, P. Book of Abstracts, ESEAC'98, Coimbra, Portugal, June 1998.
(8) Trevani, L. N.; Calvo, E.; Corti, H. R. *J. Chem. Soc., Faraday Trans.* **1997**, *93*, 4319.
(9) Liu, C.; Snyder, S. R.; Bard, A. J. *J. Phys. Chem. B* **1997**, *101*, 1180.
(10) Flarsheim, W. M.; Tsou, Y. M.; Tractenberg, I.; Johnson, K. P.; Bard, A. J. *J. Phys. Chem.* **1986**, *90*, 3857.
(11) Flarsheim, W. M.; Tsou, Y. M.; Tractenberg, I.; Johnson, K. P.; Bard, A. J. *J. Phys. Chem.* **1986**, *90*, 196.
(12) Curtiss, L. A.; Halley, J. W.; Hautman, J.; Hung, N. C.; Nagy, Z.; Rhee, Y. J.; Yonco, R. M. *J. Electrochem. Soc*. **1991**, *138*, 2032.
(13) Sharp, P. *Electrochim. Acta* **1983**, *28*, 301.
(14) Fernández, H.; Zón, M. A. *J. Electroanal. Chem*. **1992**, *332*, 237.
(15) Fernández, H.; Zón, M. A. *J. Electroanal. Chem.* **1990**, *283*, 251.
(16) Zón, M. A.; Fernández, H.; Sereno, L.; Silber, J. J. *Electrochim. Acta* **1987**, *32*, 71.
(17) Buchanan, R. M.; Calabrese, G. S.; Sobieralski, T. J.; Wrighton, M. S. *J. Electroanal. Chem.* **1983**, *153*, 129.
(18) Jeanmaire, D. L.; Van Duyne, R. P. *J. Electroanal. Chem.* **1975**, *66*, 235.
(19) Seo, E. T.; Nelson, R. F.; Fritsch, J. M.; Marcoux, L. S.; Leedy, D. W.; Adams, R. N. *J. Am. Chem. Soc.* **1966**, *88*, 3498.
(20) Nelson, R. F.; Adams, R. N. *J. Am. Chem. Soc.* **1968**, *90*, 3925.
(21) Compton, R. G.; Laing, M. E. *J. Chem. Soc., Chem. Commun.* **1988**, 1320.
(22) Moressi, M. B.; Fernández, H. *J. Electroanal. Chem.* **1994**, *369*, 153.
(23) Nelson, R. F.; Carpenter, A. K.; Seo, E. T. *J. Electrochem. Soc.* **1973**, *120*, 206.
(24) Kitagawa, T.; Layloff, T. P.; Adams, R. N. *Anal. Chem.* **1963**, *35*, 1086.
(25) Adams, R. N. *J. Electroanal. Chem.* **1964**, *8*, 151.
(26) Fujinaga, T.; Deguchi, Y.; Umemoto, K. *Chem. Soc. Jpn.* **1964**, *37*, 822.
(27) Wipf, D. O.; Wightman, R. M. *J. Phys. Chem.* **1989**, *93*, 4286.
(28) Andrieux, C. P.; Delgado, G.; Savéant, J. M. *J. Electroanal. Chem.* **1993**, *348*, 123.
(29) Parker, V. D. *Acta Chem. Scand. B* **1981**, *35*, 655.
(30) Compton, R. G.; Wellington, R. G.; Dobson, P. J.; Leigh, P. A. *J. Electroanal. Chem.* **1994**, *370*, 129.
(31) Compton, R. G.; Marken, F.; Rebbitt, T. O. *J. Chem. Soc., Chem. Commun.* **1996**, 1017.
(32) Bento, M. F.; Medeiros, M. J.; Montenegra, M. I.; Beriot, C.; Pletcher, D. *J. Electroanal. Chem.* **1993**, *345*, 273.
(33) M'Halla, F.; Pinson, J. C.; Savéant, J. M. *J. Am. Chem. Soc.* **1980**, *102*, 4120.
(34) Jaworski, J. S.; Leszczyñski, P.; Tykarski, J. *J. Chem. Res. (S)* **1995**, 510.
(35) Andrieux, C. P.; Savéant, J. M.; Zann, D. *Nouv. J. Chim.* **1984**, 107.
(36) Parker, V. D. *Acta Chem. Scand. B* **1981**, 595.
(37) Danen, W. C.; Kensler, T. K.; Lawless, J. G.; Marcus, M. F.; Hawley, M. D. *J. Phys. Chem.* **1969**, 4389.
(38) Zón, M. A.; Fernández, H.; Sereno, L.; Silber, J. *J. Electrochim. Acta* **1987**, *32*, 1733.
(39) *CRC Handbook of Chemistry and Physics*, 74th ed.; CRC Press: Cleveland, OH, 1993; pp 6−194.
(40) *CRC Handbook of Chemistry and Physics*, 74th ed.; CRC Press: Cleveland, OH 1993; pp 6−10.
(41) Wilke, C. R.; Chang, P. *AIChEJ.* **1955**, *1*, 263.
(42) Perry, J. H. *Chemical Engineers Handbook*; McGraw-Hill Book Company, Inc.: New York, 1950.
(43) Fleischmann, M.; Lasserre, F.; Robinson, J. *J. Electroanal. Chem.* **1984**, *177*, 115.
(44) Pilling, M. J.; Seakins, P. W. *Reaction Kinetics*; Oxford Science Publications: New York, 1995.